JOURNAL OF GEOPHYSICAL RESEARCH, VOL. 107, NO. D19, 4396, doi:10.1029/2001JD001309, 2002

Estimate of top-of-atmosphere albedo for a molecular atmosphere over ocean using Clouds and the Earth's Radiant Energy System measurements

Seiji Kato and Norman G. Loeb
Center for Atmospheric Sciences, Hampton University, Hampton, Virginia, USA

C. Ken Rutledge
Analytical Services & Materials, Inc., Hampton, Virginia, USA

Received 19 September 2001; revised 30 January 2002; accepted 20 February 2002; published 10 October 2002.

[1] The shortwave broadband albedo at the top of a molecular atmosphere over ocean between 40°N and 40°S is estimated using radiance measurements from the Clouds and the Earth's Radiant Energy System (CERES) instrument and the Visible Infrared Scanner (VIRS) aboard the Tropical Rainfall Measuring Mission satellite. The albedo monotonically increases from 0.059 at a solar zenith angle of 10° to 0.107 at a solar zenith angle of 60°. The estimated uncertainty in the albedo is 3.5×10^{-3} caused by the uncertainty in CERES-derived irradiances, uncertainty in VIRS-derived aerosol optical thicknesses, variations in surface wind speed and variations in ozone and water vapor. The estimated uncertainty is similar in magnitude to the standard deviation of 0.003 that is derived from 72 areas which are divided by 20° latitude by 20° longitude grid boxes. The empirically estimated albedo is compared with the modeled albedo using a radiative transfer model combined with an ocean surface bidirectional reflectivity model. The modeled albedo with standard tropical atmosphere is 0.061 and 0.111 at the solar zenith angles of 10° and 60°, respectively. The empirically estimated albedo can be used to estimate the direct radiative effect of aerosols at the top of the atmosphere over oceans. *INDEX TERMS:* 0305 Atmospheric Composition and Structure: Aerosols and particles (0345, 4801); 1640 Global Change: Remote sensing; 3359 Meteorology and Atmospheric Dynamics: Radiative processes; 4552 Oceanography: Physical: Ocean optics; *KEYWORDS:* aerosol radiative forcing, ocean surface reflectance, planetary albedo, molecular atmosphere

Citation: Kato, S., N. G. Loeb, and C. K. Rutledge, Estimate of top-of-atmosphere albedo for a molecular atmosphere over ocean using Clouds and the Earth's Radiant Energy System measurements, *J. Geophys. Res.*, *107*(D19), 4396, doi:10.1029/2001JD001309, 2002.

1. Introduction

[2] Estimating the direct radiative effect of aerosols at the top of the atmosphere from narrowband radiance measurements is difficult because uncertainties in particle size distributions, constituents, and shapes are large. Also, an increase in radiance due to scattering by particles can be similar in magnitude to variations in reflected radiance by the underlining surface. As a consequence, the uncertainty in theoretically estimated radiative effects based on retrieved aerosol optical properties can be large. An alternative method for estimating the direct aerosol radiative effect at the top of the atmosphere is to use broadband radiance measurements from a satellite [*Haywood et al.*, 1999; *Li et al.*, 2000; *Satheesh and Ramanathan*, 2000]. These measured radiances, combined with clear-sky scene identification, are used to construct angular distribution models, which provide irradiances from radiance measurements [*Loeb and Kato*, 2002]. The direct radiative effect of aerosols at the top of the atmosphere then can be defined as the difference of the albedo derived using angular distribution models from the albedo of a molecular atmosphere. The purpose of this paper is (1) to empirically estimate the globally averaged shortwave broadband top of the atmosphere albedo for a molecular atmosphere overlying a non-Lambertian ocean surface using radiance measurements at the top of the atmosphere and (2) compare it with theoretical computations by a radiative transfer model.

[3] In earlier studies, researchers computed radiances and irradiances in an ocean-atmosphere system. *Plass and Kattawar* [1968] used a Monte Carlo model to compute radiance for an ocean-atmosphere system with a smooth ocean surface. *Raschke* [1972] used a two-layer atmosphere-ocean system in which the ocean-atmosphere interface is treated by a Gaussian distribution of wave slopes [*Cox and Munk*, 1955]. *Nakajima and Tanaka* [1983] investigated the wind speed dependence of albedo in an ocean-atmosphere system and found that the albedo at the surface decreases with increasing wind speed. Polarization

0148-0227/02/2001JD001309$09.00

is treated in some models [e.g., *Fraser and Walker*, 1968; *Ahmad and Fraser*, 1982; *Takashima and Masuda*, 1985; *Kattawar and Adams*, 1989; *Wauben et al.*, 1994], while it is neglected in other models [e.g., *Tanaka and Nakajima*, 1977; *Jin and Stamnes*, 1994; *Fell and Fischer*, 2001]. *Mishchenko et al.* [1994] and *Lacis et al.* [1998] investigated the effect of neglecting polarization in radiance and irradiance computations. *Lacis et al.* [1998] show that neglecting polarization introduces less than a 1% error in the irradiance computation in an ocean-atmosphere system.

[4] In this paper, we compare the empirically derived broadband shortwave albedo of a molecular atmosphere from radiance measurements over clear-sky ocean at the top of the atmosphere with that computed by a radiative transfer model. If they agree, the albedo for a molecular atmosphere and its uncertainty provide a useful constraint in estimating the radiative effect of aerosols at the top of the atmosphere. In addition, the agreement increases the confidence level of both the data and radiative transfer model used for the comparison.

2. Determination of Albedo for a Molecular Atmosphere From Ceres-Virs Data Set

2.1. CERES-VIRS Data

[5] The Clouds and the Earth's Radiant Energy System (CERES) [*Wielicki et al.*, 1996] instrument on the Tropical Rainfall Measuring Mission (TRMM) satellite measured broadband shortwave radiances at approximately 350 km altitude at wide range of solar zenith, viewing zenith and viewing azimuth angles between 40°N and 40°S. The CERES instrument footprint size is approximately 10 km at the nadir. The Visible Infrared Scanner (VIRS), which is a five-channel imaging spectroradiometer, is also on the TRMM satellite [*Kummerow et al.*, 1998]. VIRS has a pixel size of approximately 2 km at the nadir and scans the viewing zenith angle of 0° to 45°. VIRS pixels are colocated with CERES footprints so that each CERES footprint scene can be identified using the higher-resolution VIRS measurements. CERES and VIRS colocated data along with aerosol and cloud properties derived from VIRS are available on the CERES Single Scanner Footprint product, which are used in this study.

[6] In order to avoid using footprints that contain a large unidentified scene area, only footprints for which VIRS coverage is greater than 60% were used in this study. After unfiltering CERES radiances [*Loeb et al.*, 2001] clear-sky irradiances were computed from CERES radiance using angular distribution models that depend on surface wind speed and that include effects of variation in the aerosol optical thickness [*Loeb and Kato*, 2002]. Note that the effect of the spherical earth [*Loeb et al.*, 2002] is not included in irradiances used in this study. VIRS-derived aerosol optical thicknesses within a CERES footprint were averaged using the CERES point spread function as a weighting function. In this study, we only used CERES footprints that contain more than 50% of a point spread function weighted area contributed to compute the average aerosol optical thickness over the footprint. In other words, all CERES footprints used in this study contain at least 50% weighted area covered by VIRS pixels that were used to retrieve the aerosol optical thickness.

[7] *Ignatov and Stowe* [2000] retrieved the aerosol optical thickness over CERES footprints using the VIRS 0.63 μm channel after identifying clear-sky footprints [*Minnis et al.*, 1999; *Stowe et al.*, 1999; *Trepte et al.*, 1999]. In the retrieval algorithm, *Ignatov and Stowe* [2000] assumed nonabsorbing particles having a lognormal distribution with a median radius and geometric standard deviation of 0.1 μm and 2.03, respectively. They treated ocean surface reflection using two components, one with isotropic reflection and the other with Fresnel's reflection [*Ignatov et al.*, 1995].

2.2. Empirical Estimate of Albedo for a Molecular Atmosphere

[8] In order to estimate the albedo for a molecular atmosphere from the CERES-VIRS data set, the area between latitude of 40°N and 40°S was first divided into 72 areas by 20° latitude by 20° longitude grids (Figure 1). Second, we averaged instantaneous aerosol optical thicknesses derived from VIRS radiance measurements and irradiances derived from CERES radiance measurements taken within an hour in each grid box. These averaged irradiances and aerosol optical thicknesses from 72 grid boxes are assumed to be independent. Third, we obtained a linear relationship between the averaged top of the atmosphere albedo estimated from CERES radiance measurements and averaged VIRS-derived aerosol optical thickness using the least square fitting method for each grid box. Since albedo is a function of solar zenith angle, we performed this regression for every 1° solar zenith angle increment (Figure 2). The intercept of the regression line then represents the top of the atmosphere albedo for a molecular atmosphere at each solar zenith angle. We therefore implicitly assume that the aerosol optical thickness and surface albedo are small so that the albedo at the top of the atmosphere increases linearly with optical thickness.

[9] While the intercept is not affected by the assumption of the aerosol model used in the retrieval, the slope depends on the assumptions. For example, if actual particles are absorbing, the retrieved optical thickness based on nonabsorbing particles is smaller than the actual aerosol optical thickness. Consequently, the slope will be larger than the actual slope, provided other properties are the same. In addition, both the slope and intercept are affected by calibration of instruments, cloud contaminations, variations in ozone and water vapor amounts, and surface optical properties. We address these effects on the albedo estimate in following sections. Despite these unknowns, the intercept as a function of the solar zenith angle is a smooth curve increasing from 0.059 at the solar zenith angle of 10° to 0.107 at 60° (Figure 3). The average standard deviation of the albedo derived from these 72 intercepts at solar zenith angles between 10° and 70° is 0.003. A polynomial fit to the albedo given by intercepts as a function of the solar zenith angle is

$$a = \sum_{i=0}^{4} C_i x^i, \tag{1}$$

where

$$x = \frac{\theta_0 - 0.5(\theta_2 + \theta_1)}{0.5(\theta_2 - \theta_1)}. \tag{2}$$

In these expressions a is the top-of-atmosphere albedo, θ_0 is the solar zenith angle in degrees, θ_1 and θ_2 are 0° and 69.5°,

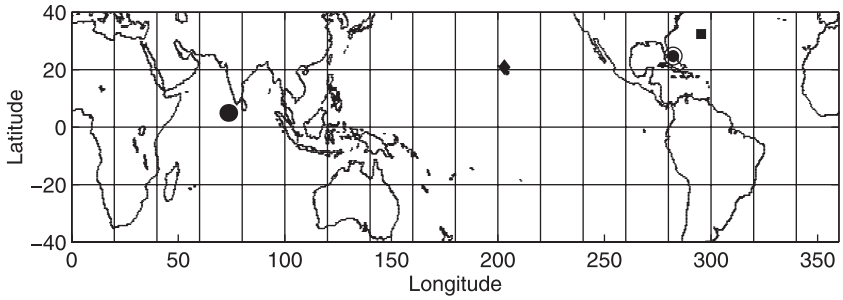

Figure 1. The 72 areas between 40°N and 40°S divided by 20° latitude and 20° longitude grid boxes. Also provided are the location of four Aerosol Robotic Network (AERONET) sites: Kaashodhoo (solid circle), Bermuda (square), Andros Island (open and solid circle), and Lanai (diamond).

respectively, and C_i is the coefficient determined by the fitting. The values of C_i computed by a Chebyshev approximation [*Press et al.*, 1992] is listed in Table 1. The residual variance of the fit from intercepts is 8.2×10^{-7}.

3. Error Analysis and Sensitivity Study of the Empirically Derived Albedo

[10] The error in the empirically estimated albedo of a molecular atmosphere given by (1) is caused by the error in CERES-derived irradiances and in VIRS-derived aerosol optical thickness. The former is caused by the error in angular distribution models and calibration of the CERES instrument. The latter is caused by assumptions in the retrieval algorithm and the VIRS calibration. If the clear-sky identification by VIRS instrument has errors, it cause errors in both CERES-derived irradiances and VIRS-derived aerosol optical thicknesses since scene identification by VIRS is also used in building angular distribution models [*Loeb and Kato*, 2002]. We estimate errors in these

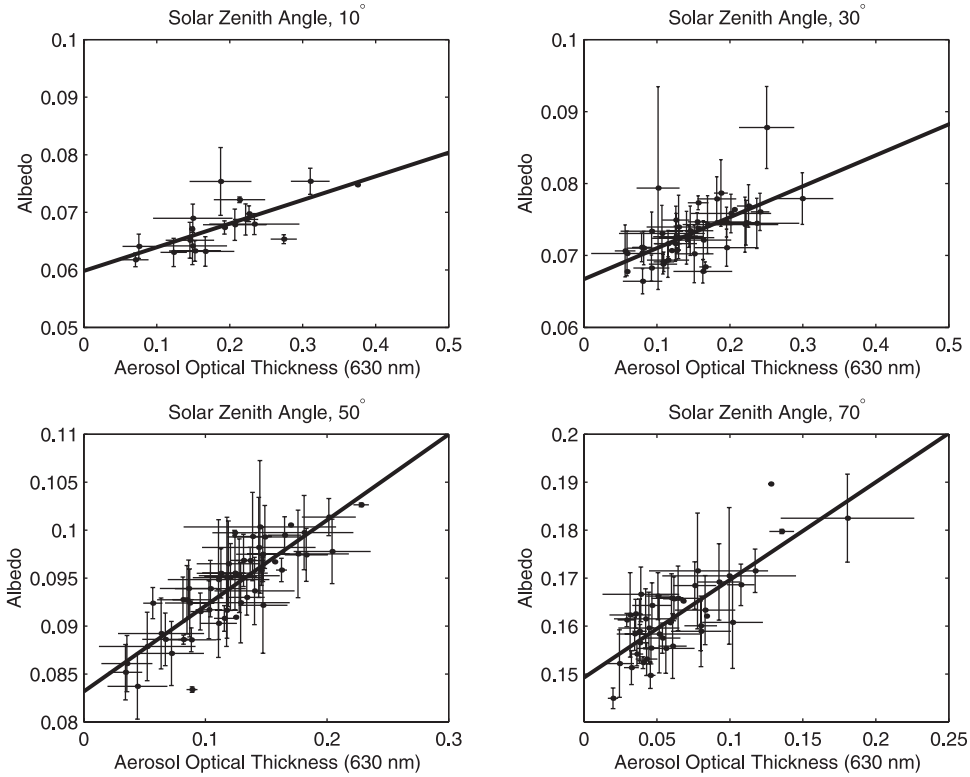

Figure 2. Albedo derived from the Clouds and Earth's Radiant Energy System (CERES) as a function of aerosol optical thickness derived from the Visible Infrared Scanner (VIRS) for 10°, 30°, 50°, and 70° solar zenith angles. Data taken in the area of 160°W < longitude 180°W and 0° < latitude < 20°N are used for the plot. The vertical and horizontal lines indicate variations in CERES-derived albedos VIRS-derived aerosol optical thicknesses measured within an hour, respectively. The thick solid line indicates the linear regression line.

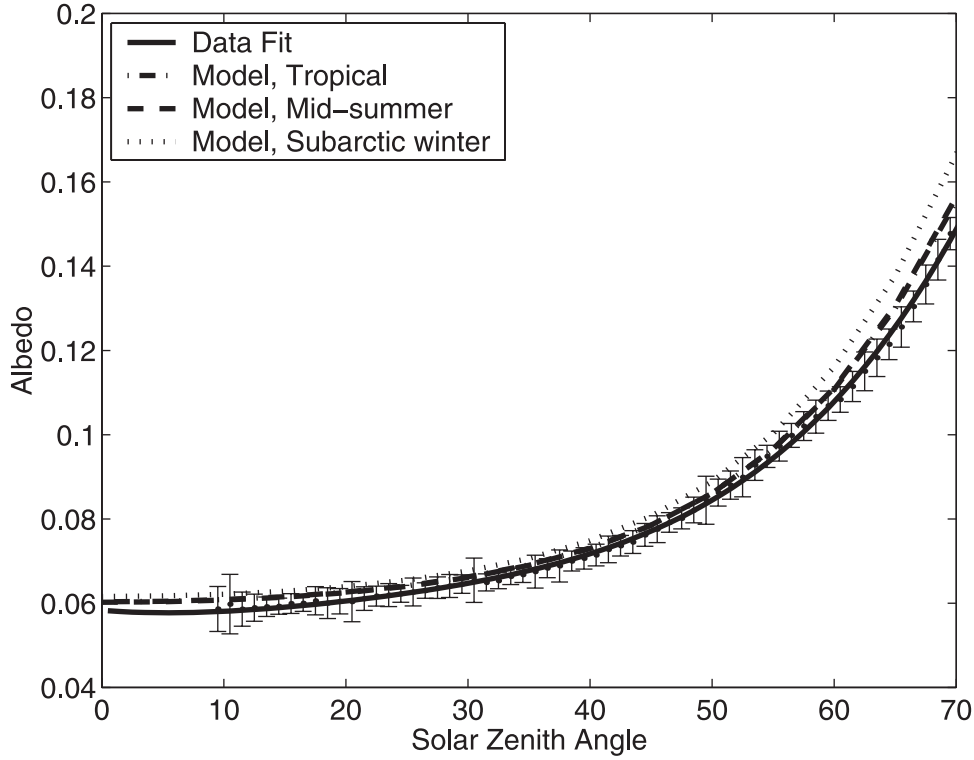

Figure 3. Top of the molecular atmosphere albedo over oceans derived from CERES and VIRS data sets as a function of solar zenith angles (solid line). Vertical lines indicate the standard deviation derived from 72 areas between 40°N and 40°S divided by 20° latitude by 20° longitude grid boxes. The dash-dot, dashed, and dotted line indicate modeled albedos with the standard tropical, midlatitude summer and subarctic winter atmospheres [*McClatchey et al.*, 1972], respectively.

derived values in the following sections and performs a sensitivity study of the albedo of a molecular atmosphere.

3.1. Uncertainty in the CERES-Derived Irradiance

[11] The error in the CERES-derived irradiance caused by the instrument calibration is 1% [*Priestley et al.*, 2000] and by conversion of filtered radiances to unfiltered radiances is also 1% [*Loeb et al.*, 2001]. *Loeb and Kato* [2002] estimate that the uncertainty in CERES-derived irradiances caused by cloud contaminations is 2%. It is difficult to estimate the error by the angular distribution model because the true irradiance is unknown. As an estimate of this error, *Loeb and Kato* [2002] use the difference between the averaged irradiance derived from angular distribution models and measured radiances integrating over viewing zenith and azimuth angles, which leads to the error by the angular distribution model of approximately 0.5%. If these errors are uncorrelated, therefore, the uncertainty in CERES-derived irradiances is approximately 2.5%.

3.2. Uncertainty in the VIRS-Derived Aerosol Optical Thickness

[12] The retrieved aerosol optical thickness from VIRS radiance measurements at 630 nm were compared with the optical thickness estimated from quality assured data (level 2.0) taken by Aerosol Robotic Network (AERONET) sun-photometers [*Holben et al.*, 1998] to evaluate the error in VIRS-derives aerosol optical thicknesses. We selected four island sites, Kaashodhoo (4.965°N, 73.466°E), Bermuda (32.370°N, 64.696°W), Andros Island (24.700°N, 77.800°W), and Lanai (20.826°N, 156.985°W) to represent ocean environment for the comparison. The VIRS-derived aerosol optical thickness averaged over a clear-sky CERES footprint within a 0.5° latitude by 0.5° longitude area centered at these sites was compared with the AERONET-derived aerosol optical thickness that was linearly interpolated in time. Since AERONET measures optical thickness at 500 nm and 670 nm, the optical thicknesses measured at these wavelengths were linearly interpolated in logarithmic space to obtain the optical thickness at 630 nm. Because VIRS takes multiple measurements within a 0.5° longitude by 0.5° latitude area from one overpass, we averaged VIRS-derived aerosol optical thickness taken within one hour in a 0.5° latitude by 0.5° longitude area. In addition, a three hour window was applied to AERONET data such that if

Table 1. Coefficients of Albedo Fitting[a]

Coefficient	Value
C_0	6.7568×10^{-2}
C_1	2.3530×10^{-2}
C_2	2.2873×10^{-2}
C_3	2.0383×10^{-2}
C_4	1.1793×10^{-2}

[a] The effect of the spherical Earth [*Loeb et al.*, 2002] is not included in this estimate.

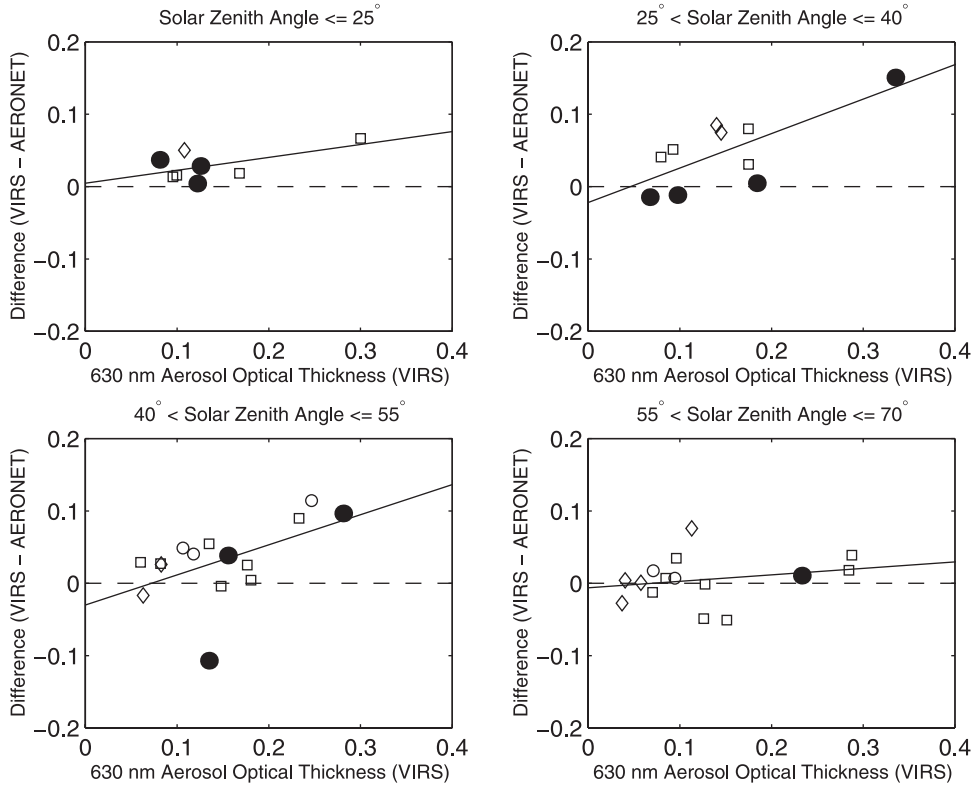

Figure 4. Difference of the VIRS-derived aerosol optical thickness from AERONET-derived aerosol optical thickness as a function of VIRS-derived aerosol optical thickness. Four AERONET island sites, Kaashodhoo (solid circle), Bermuda (square), Andros Island (open circle), and Lanai (diamond), are selected for the comparison. All sites are at the sea level. The solid and dashed lines indicate the regression line and zero line, respectively.

AERONET retrieval was not found within a ±1.5 hour period from an overpass, we did not compare the optical thicknesses. This avoids interpolations of the AERONET-derived optical thickness from two clear-periods occurring before and after a cloudy period.

[13] Figure 4 shows the comparison of VIRS- and AERONET-derived aerosol optical thicknesses separated by four solar zenith angle ranges. The difference between AERONET- and VIRS-derived aerosol optical thickness (VIRS - AERONET) are plotted as a function of VIRS-derived optical thickness. According to *Holben et al.* [2001] the uncertainty in the sun photometer-derived optical thicknesses is between 0.01 and 0.02 because of the calibration uncertainty. This uncertainty in AERONET-derived aerosol optical thicknesses is small enough for our purpose so that AERONET-derived aerosol optical thicknesses are considered to be true values in this study. Therefore, the ordinate in Figure 4 can be considered as an error in the VIRS-derived aerosol optical thickness. The error increases with optical thickness and is a function of solar zenith angle. VIRS-derived aerosol optical thicknesses are generally larger than AERONET-derived aerosol optical thicknesses. In addition, the error appears to be smaller at larger solar zenith angles (Figure 4).

3.3. Sensitivity Study of Empirically Derived Albedo

[14] We can alter CERES-derived irradiances and VIRS-derived aerosol optical thicknesses by their uncertainties to analyze the sensitivity of the empirically derived albedo for a molecular atmosphere. When the albedo computed from the CERES-derived irradiance is increased by 2.5% to perform the linear regression shown in Figure 2, the intercepts increase approximately by 0.002 (Figure 5, thin solid line), which is approximately 2.5% of the averaged albedo over solar zenith angles between 0° to 70°. In order to investigate the effect of the uncertainty in the VIRS-derived aerosol optical thickness to the albedo, we altered VIRS-derived aerosol optical thicknesses τ by

$$\tau' = (1 - \alpha)\tau - \beta, \tag{3}$$

where α and β are solar zenith angle dependent intercepts and slopes, respectively. These values used for the sensitivity study are shown in Table 2. When the aerosol optical thicknesses are altered by (3) to perform regressions between albedos and optical thicknesses similar to those shown in Figure 2, intercepts decrease for the most part of solar zenith angles; the maximum difference occurs at near the solar zenith angle of 50° (Figure 5, thick solid line). The difference shown on Figure 5 and error in the VIRS-derived aerosol optical thickness shown on Figure 4 are related. When the error in the VIRS-derived aerosol optical thickness is positive (negative) at the small value, (3) increases (decreases) the albedo. The root-mean

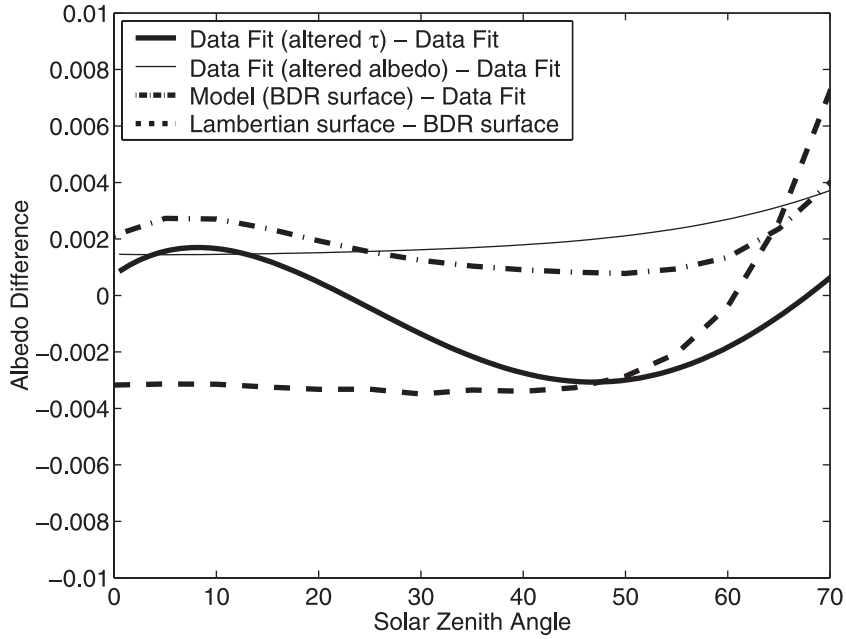

Figure 5. Difference of the top of the atmosphere albedo derived from the CERES-VIRS data set (intercepts) with altered aerosol optical thickness by equation (3) from the intercept without altering (thick solid line). The difference of the albedo with increased CERES-derived irradiances by 2.5% from that without the increase the irradiances is shown by thin solid line. The difference of modeled top of the atmosphere albedo by Discrete Ordinates Radiative Transfer (DISORT) from CERES-VIRS derived albedo without altering optical thickness and irradiance is also shown by dash-dot lines. The difference of modeled albedo with a Lambertian surface from that with a bidirectional reflectivity model is shown by dashed line.

squared difference of the albedo at the solar zenith angle between 0° to 70° is 0.0019.

4. Comparison With Radiative Transfer Model Results

[15] In this section, we compare the measurements with theoretical calculations of both irradiances and radiances for a consistency check because the agreement provides more confidence in our estimate. Since the irradiance is an integrated value over angles, the agreement of albedo can be accomplished by cancellation of the error in radiances at different angles. Comparison of radiances at different zenith and azimuth angles can identify such errors. In addition, to make the comparison more complete, it is logical to check whether the ocean bidirectional reflectivity model used for the computation gives a realistic ocean surface albedo since it provides the bottom boundary condition in the radiative transfer computation. Therefore, we also compare the ocean surface albedo used in the model with measurements. We could use, for example, a two-stream model to compute the top-of-atmosphere albedo for the comparison. As explains in the discussion section, lambertian ocean surface and two-stream assumptions, however, introduce a noticeable error in computing irradiance over the ocean surface. For this reason, we use the DISORT radiative transfer model [*Stamnes et al.*, 1988], which can incorporate an ocean bidirectional reflectivity model and compute the zenith and azimuth angle dependent radiance.

4.1. Model Description

[16] The upward radiance field over a clear-sky ocean has sharp features because of specular reflection of the direct solar radiation by the ocean surface. In order to capture the sharp features and accurately resolve the azimuthal dependence, more than a hundred terms may be needed to express the azimuth angle dependence of the radiance field in a Fourier series. This would also require more than a hundred streams in the discrete ordinate algorithm. Since multiple scattering tends to smooth out sharp features in radiance field, they are mainly caused by single scattering [*van de Hulst*, 1980; *de Hann et al.*, 1987]. Sharp features in the upward radiance at the top of the atmosphere are, therefore, mainly caused by the radiance directly transmitted after

Table 2. Estimate Error of VIRS-Derived Aerosol Optical Thickness

Solar Zenith Angle	$\theta_0 \leq 25°$	$25° < \theta_0 \leq 40°$	$40° < \theta_0 \leq 55°$	$55° < \theta_0 \leq 70°$
Mean bias	0.05	0.05	0.03	0.01
Standard deviation	0.04	0.04	0.06	0.03
Slope	0.28	0.42	0.46	0.07
Intercept	0.01	−0.01	−0.04	0.00

either single scattering by particles or reflection of the direct solar radiation by the ocean surface. DISORT adopted the algorithm of *Nakajima and Tanaka* [1988] to correct sharp features that appear in radiance field due to single scattering by particles (K. Stamnes et al., DISORT, a general-purpose Fortran program for discrete-ordinate-method radiative transfer in scattering and emitting layered media: Documentation of methodology, ftp://climate.gsfc.nasa.gov/pub/wiscombe/Multiple_Scatt/, 2000) (hereinafter cited as *Stamnes et al.*, 2000). Because of this correction, less than 10 streams are enough to compute radiances in the atmosphere if the surface reflection is not large or not highly directional [*Stamnes et al.*, 2000, p. 79]. However, DISORT does not correct errors in reflection from the surface. To correct the error in the upward radiance at the top of the atmosphere, we subtract the contribution of the directly transmitted radiance computed by insufficient Fourier terms and add the exact radiance directly transmitted from the surface. Therefore the upward radiance I at the top of the atmosphere is

$$I(\tau=0,\mu,\phi-\phi_0)=\sum_{m=0}^{2M-1} I^m(\tau=0,\mu)\cos m(\phi_0-\phi) - \frac{1}{\pi}\mu_0 F_0 \sum_{m=0}^{2M-1} e^{-(1/\mu_0+1/\mu)\tau_a}\rho_d^m(\mu,-\mu_0)\cos m(\phi_0-\phi) + \frac{1}{\pi}\mu_0 F_0 e^{-(1/\mu_0+1/\mu)\tau_a}\rho_d(\mu,-\mu_0,\phi_0-\phi), \quad (4)$$

where

$$I^m(\tau,\mu)=\frac{2-\delta_{m0}}{2\pi}\int_{-\pi}^{\pi} I(\tau,\mu,\phi)\cos m\phi\, d\phi, \quad (5)$$

$$\rho_d^m(\mu,-\mu_0)=\frac{2-\delta_{m0}}{2\pi}\int_{-\pi}^{\pi}\rho_d(\mu,-\mu_0,\phi-\phi')\cos m(\phi-\phi_0)d(\phi-\phi_0), \quad (6)$$

$$\delta_m=1 \quad (m=0), \qquad =0 \quad (m\neq 0),$$

ρ_d is the bidirectional reflectivity of the ocean surface, F_0 is the direct solar irradiance at the top of the atmosphere, μ_0 is the solar zenith angle, τ is the optical thickness of the atmosphere, and τ_a is τ measured from top of the atmosphere to the surface. The first term on the right side of equation (4) is the upward radiance at the top of the atmosphere (τ = 0) at the cosine of the zenith angle of μ and the azimuth angle of ϕ measured from the azimuth angle of the direct solar radiation of ϕ_0. The second term represents the directly transmitted radiance from the surface after the reflection of the direct solar radiation at the angle of μ_0 and ϕ_0. The second term is replaced by the third term using the exact bidirectional reflectivity of the ocean surface to correct the error caused by the Fourier series expansion of the bidirectional reflectivity in 2M terms. Note that the total number of Fourier terms $2M$ is equal to or less than the number of streams used in DISORT [*Stamnes et al.*, 2000 p. 88].

[17] We computed the top-of-atmosphere radiance for a molecular atmosphere using the correction in equation (4) with 12 streams. The standard tropical atmosphere [*McClatchey et al.*, 1972], and *k*-distribution tables with the correlated-*k* assumption given by *Kato et al.* [1999] were used to compute absorption by water vapor, ozone, carbon dioxide, and oxygen. The ocean surface bidirectional reflectivity model given by *Vermote et al.* [1997] was used to compute reflection from the ocean surface. According to E. F. Vermote et al. (6S User guide, version 2, 1997, available at ftp://loaser.univ-lillel.fr) it treats reflection from whitecaps [*Koepke*, 1984], specular reflection [*Cox and Munk*, 1954, 1955], and scattering underwater [*Morel*, 1988]. For the comparison, we used the wind speed of 5 m s^{-1} and pigment concentration of 0.01 mg m^{-3}, and salinity of 34.3 ppt.

4.2. Comparisons

[18] The modeled albedo is 0.061 and 0.111 at the solar zenith angle of 10° and 60°, respectively, while the corresponding albedos derived from the CERES-VIRS data set is 0.059 and 0.107.These modeled albedos at two solar zenith angles are 3.3% and 3.7% greater relative to those derived from the CERES-VIRS data set. Figures 3 and 5 show that the modeled albedo with both standard tropical and midlatitude atmospheres are within the standard deviation of albedo (0.003) derived from the CERES-VIRS data set. When the modeled upward irradiance at the top of the atmosphere for a molecular atmosphere with the standard tropical, midlatitude summer and sub-arctic winter atmospheres are averaged over solar zenith angles between 0° and 70°, they are 2.3 W m^{-2}, 2.3 W m^{-2}, and 4.7 W m^{-2}, respectively, greater than the upward irradiance obtained from the fitting by equation (1) multiplied by the downward irradiance at the top of the atmosphere.

[19] In order to compare modeled radiances with CERES measurements, we limited CERES measurements in the area of 0° < latitude < 40°S and 90°W < longitude < 130°W to select radiances measured at low aerosol loading conditions. All CERES radiances measured over the region were sorted into 5° solar zenith, viewing zenith and azimuth angle bins to obtain the average radiance at each angle. The averaged VIRS-derived aerosol optical thickness in this region for 9 months is 0.074. Figure 6 shows the comparison of measured and modeled radiances with no aerosol and with ammonium sulfate particles. The optical thickness of ammonium sulfate particles used in the computation is 0.1. We assumed the median radius and standard deviation of 0.1 and 2.03 of lognormal distribution, respectively, for particles, which is the same size distribution used in the retrieval algorithm. Optical properties of particles were computed using Mie theory and refractive indices of ammonium sulfate given by *Toon and Pollack* [1976]. Figure 6 shows that CERES radiances are between modeled radiances with and without aerosols for most of the angles, which is what we expect since the average aerosol optical thickness over the region is 0.074. CERES radiances are, however, closer to radiances with no aerosol. Since our result shows that the VIRS-derived aerosol optical thickness tends to be larger compared with the AERONET-derived aerosol optical thickness, the average aerosol optical thickness of 0.074 might be overestimated by the retrieval.

4.3. Comparison With Ocean Surface Albedo Measurements With 6S Ocean Surface Model

[20] The NASA Langley Research Center Radiation and Aerosols Branch surface measurement group took ocean albedo measurements at the Chesapeake Bay lighthouse

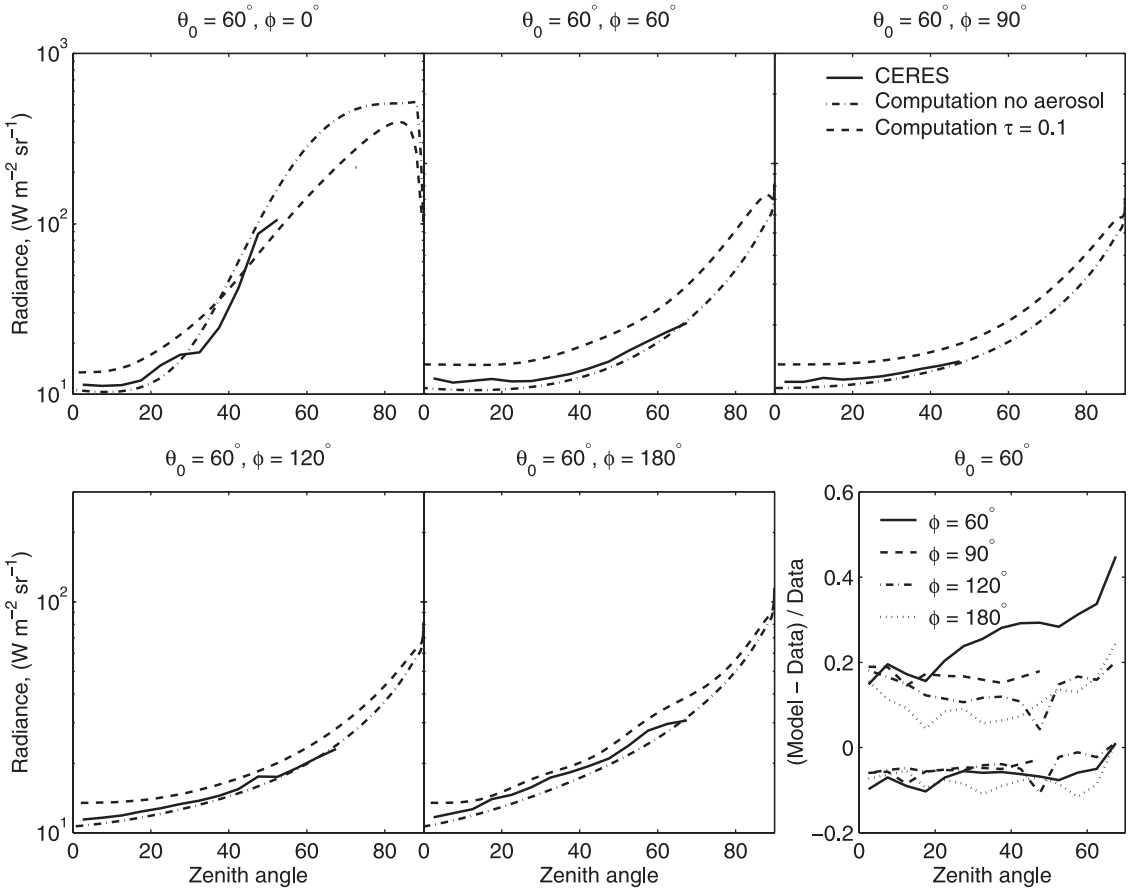

Figure 6. Comparison of averaged radiances measured by CERES (solid line) in the area of 0° < latitude < 40°S and 90°W < longitude < 130°W with modeled radiance with no aerosol (dash-dot line) and with aerosol (dashed line). CERES radiances are averaged by sorting into 5° angular bins. The averaged optical thickness of the area is 0.074. The aerosol optical thickness of 0.1 is used in the model. The relative difference with (top set of lines) and without (bottom set of lines) aerosols is shown on the bottom left plot.

(36.9°N, 75.71°W), which is located approximately 25 km east of Virginia Beach. The seawater depth at the lighthouse is about 11 m. Albedos were measured at 20 m above the sea surface from March 2000 to March2001. Albedos measured under clear-sky conditions were selected using the clear-sky identification algorithm of *Long and Ackerman* [2000]. Note that only afternoon data were considered to avoid shading by the lighthouse in the field of view of the downward looking pyranometer. The modeled ocean surface albedo with wind speed of 5 m s^{-1} is lower than most of the measurements (Figure 7). Measured albedos that are less than theoretical estimate around solar zenith angles of 60° to 80° are likely to be those measured under cloudy sky conditions for the following reason. The albedo becomes a weak function of the solar zenith angle as the diffuse component of the downward irradiance at the surface increases because of reduction of specular reflection. Since estimating cloud fraction from broadband direct and diffuse measurements at large solar zenith angles is difficult, the error in estimating cloud fraction by the *Long and Ackerman* [2000] algorithm appears to be the cause of these lower albedos at low solar zenith angles. When measured ocean surface upward irradiances are sorted into one degree solar zenith angle bins and averaged over all available solar zenith angles, measured irradiances are 2.8 W m^{-2} greater than modeled ocean surface albedo multiplied by the downward irradiance computed with the standard tropical atmosphere and with no aerosol. Since coastal waters contains more particles than deep waters, this difference might be caused by scattering by particles in coastal waters (Z. Jin, personal communication, 2001).

[21] Even though albedos measured at the lighthouse might not represent the albedo of deep waters, they should provide a reasonable range of albedos corresponding to the variation of wind speeds. In order to determine the albedo as a function of wind speed, first, measured ocean surface albedos were separated into three wind speed ranges. Second, ocean surface albedos in each wind speed range were averaged to obtain the averaged value $\hat{a}(\mu_0)$A, as a function of solar zenith angle. Third, the albedo $\bar{a}(\mu_0)$ that is the average albedo including all three wind speed ranges was subtracted from $\hat{a}(\mu_0)$. Figure 8 shows the difference from the overall average, $\hat{a} - \bar{a}$, as a function of solar zenith angle for each wind speed range by open circles. The thick solid line indicates a polynomial fit to the difference. The measured albedo difference shows a weak dependence on

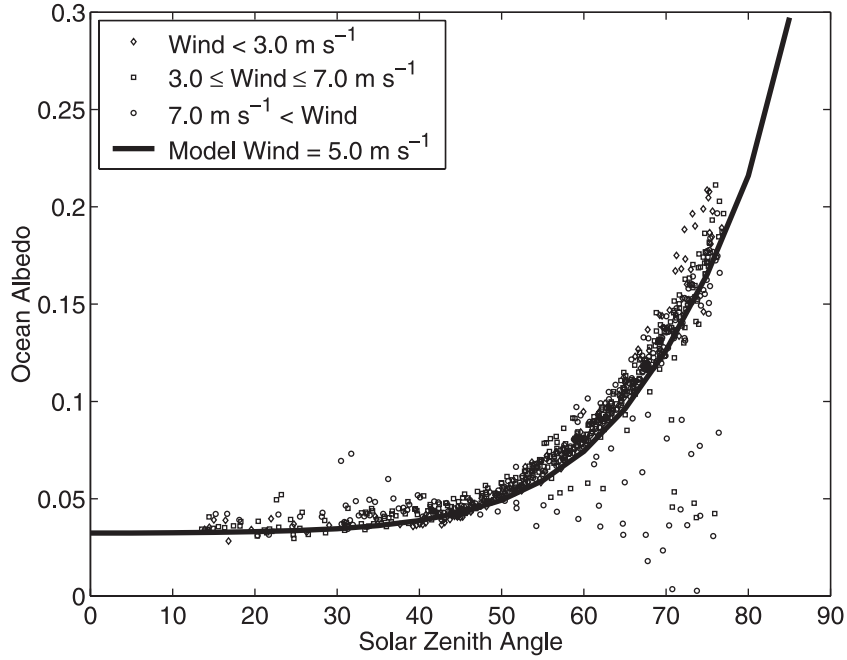

Figure 7. Measured ocean surface albedo under clear-sky conditions at the Chesapeake Bay lighthouse separated by three wind speed ranges, less than 3 m s^{-1} (diamond), between 3 m s^{-1} and 7 m s^{-1} (square) and greater than 7 m s^{-1} (circle). The solid line indicates the modeled albedo by the ocean bidirectional reflectivity model given by *Vermote et al.* [1997]. Here 5 m s^{-1} wind speed was used in the computation.

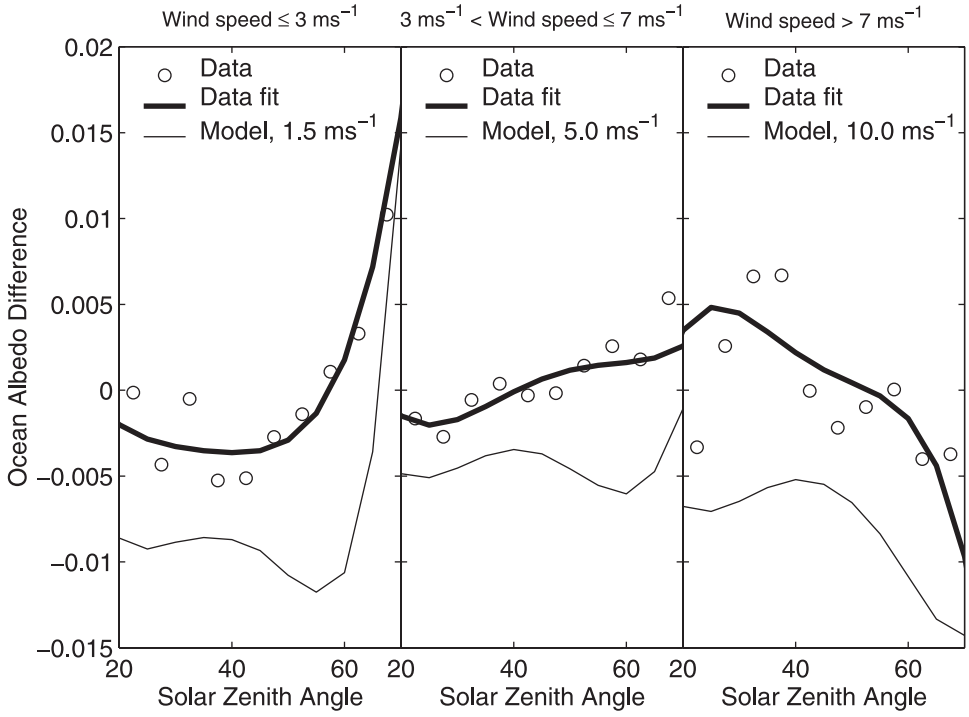

Figure 8. Difference of wind speed dependent ocean surface albedos $\hat{a}$ from the average albedo $\bar{a}$ as a function of solar zenith angle. Wind speeds are separated into three ranges, less than 3 m s^{-1}, between 3 m s^{-1} and 7 m s^{-1}, and greater than 7 m s^{-1} to compute the wind speed-dependent average albedo $\hat{a}$. The average albedo $\bar{a}$ is determined from data (Figure 7) including all wind speeds. The differences $\hat{a} - \bar{a}$ are also fitted by a polynomial (thick solid line). The thin solid lines indicate the difference of the modeled albedo by the ocean bidirectional reflectivity model of *Vermote et al.* [1997] from the average albedo $\bar{a}$.

wind speed for less than 7 m s^{-1} and the solar zenith angles less than 60°. The albedo increases by up to approximately 0.005 when the wind speed exceed 7 m s^{-1} for solar zenith angle less than 40° (Figure 8). Figure 8 also shows that increasing wind speed reduces the albedo for solar zenith angles greater than approximately 55°. When wind speed increases, both ocean surface roughness and whitecaps coverage increase. Increasing the ocean surface roughness tends to reduce the albedo [*Nakajima and Tanaka*, 1983], whereas an increase in whitecap coverage increases albedo [*Gordon and Jacobs*, 1977]. The data show that the whitecap effect dominates at the solar zenith angle less than 50° to 60° and the surface roughness effect dominates at greater solar zenith angles. The albedo computed by the ocean bidirectional reflectivity model given by *Vermote et al.* [1997] shows a similar solar zenith dependence with measurements at large solar zenith angles for each wind speed range while the magnitude of variation is about a half at the solar zenith angles approximately less than 30°.

4.4. Sensitivity of Albedo to Wind Speed

[22] Comparison of modeled ocean surface albedo with measurements in the previous section indicates that the model provides a realistic wind speed dependence. Therefore we used the model for a sensitivity study by changing the surface wind speed from 5 m s^{-1} to 2 m s^{-1} and to 10 m s^{-1} to compute the albedo change at the top of the atmosphere. Based on wind speed estimate included in 9 months of the CERES Single Scanner Footprint product, approximately 10% and 4% of footprints have the mean wind speed below 2 m s^{-1} and above 10 m s^{-1}, respectively, over oceans between 40°N and 40°S. The average wind speed for the same area is 5.6 m s^{-1}. The root-mean-square difference of the albedo with the wind speed of 2 and 10 m s^{-1} from 5 m s^{-1} at solar zenith angles between 0° to70° is 0.0024 and 0.0021, respectively.

5. Discussion

[23] As mentioned earlier, the uncertainty in AERONET-derived aerosol optical thicknesses is between 0.01 and 0.02 [*Holben et al.*, 2001]. If we assume that the asymmetry parameter of particles, g, is 0.6 and that the fraction of light scattered in the backward hemisphere is approximately given by $0.5-0.5g$ [*Twomey*, 1977], the top-of-atmosphere albedo increases approximately 0.002 by 0.01 increase in the aerosol optical thickness of nonabsorbing particles. The uncertainty in the empirically estimated albedo of a molecular atmosphere caused by the uncertainty in VIRS-derived aerosol optical thickness is about the same magnitude even though the uncertainty in the VIRS-derived optical thickness is larger than 0.01. An important condition to achieve a small uncertainty in the empirically derived albedo of a molecular atmosphere is that the errors in the VIRS-derived aerosol optical thickness and CERES-derived irradiance approach zero when the aerosol optical thickness approaches zero. Figure 4 demonstrates that, on average, the error in the VIRS-derived aerosol optical thickness is small when the values are close to zero.

[24] In the radiative transfer model, we neglect state of polarization to compute the top of the atmosphere albedo. Since the incident solar radiation at the top of the atmosphere is not polarized, it does not introduce an error in computing single scattered light. Because light is partially polarized on reflection by ocean surface and scattering by molecules, neglecting state of polarization introduces an error computing multiple scattering by molecules. An error is also introduced in treating reflection of the ocean surface illuminated by partially polarized diffuse light if polarization is neglected. *Lacis et al.* [1998] investigated the magnitude of the error and showed that the error in the upward radiance at the top of the atmosphere can be up to 10% (relative) for monochromatic light; neglecting polarization in the model tends to under estimate the radiance over the ocean surface at the azimuth angle relative to the direct solar radiation greater than 90° (backward direction). The error in the albedo is, however, less than 1% (relative) due to cancellation of errors in the radiance at different angles. In addition, the agreement shown in Figure 6 indicates that the error caused by neglecting polarization in broadband radiance computation might not be large.

[25] We analyzed the uncertainty in the empirically derived albedo of a molecular atmosphere caused by the error in CERES-derived irradiances and in VIRS-derived aerosol optical thicknesses, variation of ozone and water vapor amounts, and variation of the surface wind speed. Both uncertainties in CERES-derived irradiances and VIRS-derived aerosol optical thicknesses cause 0.002 albedo uncertainty, if we take the root-mean-square difference at solar zenith angles between 0° and 70° as the uncertainty. This corresponds to approximately 0.7 W m^{-2} difference in the daily averaged irradiance. The uncertainty in the albedo over tropical and midlatitude ocean caused by variation of water vapor and ozone is negligible. Wind speed ranging from 2 m s^{-1} to 10 m s^{-1} caused 0.002 albedo difference, which also corresponds to approximately 0.7 W m^{-2} in the daily averaged irradiance. Note that the average wind speed over oceans between 40°N and 40°S is close to 5 m s^{-1} and about 15% of CERES footprints fall outside the 2 to 10 m s^{-1} wind speed range. If errors caused by these four factors are uncorrelated, the uncertainty is approximately 3.5×10^{-3} in albedo, which corresponds to 1.2 W m^{-2} in the daily averaged irradiance. This estimated uncertainty is similar in magnitude to the standard deviation of 0.003 derived from 72 areas. This implies that the errors in CERES-derived irradiances, VIRS-derived aerosol optical thicknesses, and variation in wind speed are the major source of uncertainty in the empirically estimated albedo of a molecular atmosphere for a given solar zenith angle. In addition, the theoretical estimate of albedo for a molecular atmosphere is within the standard deviation of 0.003 for the solar zenith angle less than 70°.

[26] Earlier, we briefly mentioned that a two-stream model can introduce a noticeable error in the irradiance from an ocean surface. When the lower boundary condition is constrained by the surface albedo and uses a two-stream radiative transfer model, Figure 5 shows that it introduces an error in computing the albedo at the top of the atmosphere. The difference depends on the solar zenith angle; a two-stream approximation provides smaller (larger) irradiances when the solar zenith angle is less (greater) than 60°. The two-stream approximation underestimates the albedo by 0.003 when the solar zenith angle is less than 50°. The

difference can be qualitatively understood using a single-layer two stream model; the transmittance of the collimated beam incident on a molecular layer is larger (smaller) than the transmittance of diffuse illumination on the layer when the solar zenith angle is small (large) [e.g., *Meador and Weaver*, 1980]. Therefore, using Lambertian surface and computing irradiances in the atmosphere with a two-stream approximation instead of using the bidirectional reflectivity of the ocean surface and computing radiances provides a smaller (larger) upward irradiance at the top of the atmosphere when the solar zenith angle is small (large).

6. Conclusion

[27] We empirically and theoretically derived the top-of-atmosphere albedo for a molecular atmosphere. The albedo for a molecular atmosphere estimated from CERES-VIRS data monotonically increases from 0.059 at the solar zenith angle of 10° to 0.107 at the solar zenith angle of 60°. The standard deviation of the albedo derived from 72 areas between 40°N and 40°S divided by 20° latitude by 20° longitude grid boxes is 0.003. This is equivalent to 1.0 W m^{-2} in the daily averaged irradiance. When CERES-derived irradiances and VIRS-derived aerosol optical thickness is altered within their uncertainty, the empirically derived albedo increases approximately by 0.002 for both cases. The uncertainty in the empirically derived albedo caused by the difference in ozone and water vapor amounts between tropical and midlatitude summer standard atmospheres is negligible and the uncertainty caused by the variation in the surface wind speed is 0.002. The total uncertainty in the albedo caused by these four factors is 3.5×10^{-3}, which corresponds to 1.2 W m^{-2} in the daily average irradiance.

[28] In order to determine the uncertainty in VIRS-derived aerosol optical thicknesses, we compared them with AERONET-derived aerosol optical thicknesses. The difference depends on the solar zenith angle. While VIRS-derived aerosol optical thicknesses are generally larger than AERONET-derived aerosol optical thicknesses, the error approaches zero as the optical thickness approach zero.

[29] We also compared ocean surface albedo computed by a bidirectional reflectivity model given by *Vermote et al.* [1997] with measurements taken at the Chesapeake Bay lighthouse. While the modeled albedo is approximately 0.005 smaller than the measurements at the solar zenith angle between 20° and 70° probably because of the abundance of particles in coastal waters, the modeled albedo shows a similar wind speed dependence for a given solar zenith angle. The measurements indicate that the ocean surface albedo varies ±0.005 depending on the wind speed. The albedo increases with wind speed at the solar zenith angle less than approximately 55° and decreases with wind speed at greater solar zenith angles.

[30] **Acknowledgments.** We thank B. N. Holben, C. McLain at NASA Goddard Space Flight Center, and Goddard's AERONET staff for supplying AERONET data; B. Cairns at Colombia university and F. K. Evans at University of Colorado for suggestions on modeling radiances over oceans; T. P Charlock at NASA Langley Research Center and Z. Jin at Analytical Services & Materials for discussions regarding ocean bidirectional reflectivity; and J. A. Coakley Jr. at Oregon State University for discussions on determining the error in aerosol optical thicknesses. We also thank A. Ignatov at NOAANESDIS, who provided many constructive comments, which significantly improved the manuscript. The work is supported by the Clouds and the Earth's Radiant Energy System (CERES) project under NASA grant (NAG-1-2318).

References

Ahmad, Z., and R. S. Fraser, An iterative radiative transfer code for ocean-atmosphere systems, *J. Atmos. Sci.*, *39*, 656–665, 1982.

Cox, C., and W. Munk, Measurement of the roughness of the sea surface from photographs of the Sun's glitter, *J. Opt. Soc. Am.*, *44*, 838–850, 1954.

Cox, C., and W. Munk, Some problems in optical oceanography, *J. Mar. Res.*, *14*, 63–78, 1955.

de Hann, J. F., P. B. Bosma, and J. W. Hovenier, The adding method for multiple scattering calculations of polarized light, *Astron. Astrophys.*, *183*, 371–391, 1987.

Fell, F., and J. Fischer, Numerical simulation of the light field in the atmosphere-ocean system using the matrix-operator method, *J. Quant. Spectrosc. Radiat. Transfer*, *69*, 351–388, 2001.

Fraser, R. S., and W. H. Walker, The effect of specular reflection at the ground on light scattered from Rayleigh atmosphere, *J. Opt. Soc. Am.*, *58*, 636–644, 1968.

Gordon, H., and M. M. Jacobs, Albedo of the ocean-atmosphere system: Influence of sea form, *Appl.*, *16*, 2257–2260, 1977.

Haywood, J. M., V. Ramaswamy, and B. J. Soden, Tropospheric aerosol climate forcing in clear-sky satellite observations over oceans, *Science*, *283*, 1299–1303, 1999.

Holben, B. N., et al., AERONET—A federated instrument network and data archive for aerosol characterization, *Remote Sens. Environ.*, *66*, 1–16, 1998.

Holben, B. N., et al., An emerging ground-based aerosol climatology: Aerosol optical depth from AERONET, *J. Geophys. Res.*, *106*, 12,067–12,097, 2001.

Ignatov, A. M., and L. L. Stowe, Physical basis, premises, and self-consistency checks of aerosol retrievals from TRMM/VIRS, *J. Appl. Meteorol.*, *39*, 2259–2277, 2000.

Ignatov, A. M., L. L. Stowe, S. M. Sakerin, and G. K. Korotaev, Validation of the NOAA/NESDIS satellite aerosol product over the North Atlantic in 1989, *J. Geophys. Res.*, *100*, 5123–5132, 1995.

Jin, Z., and K. Stamnes, Radiative transfer in nonuniformly refracting layered media: Atmosphere-ocean system, *Appl. Opt.*, *33*, 431–441, 1994.

Kato, S., T. P. Ackerman, J. H. Mather, and E. E. Clothiaux, The *k*-distribution method and correlated-*k* approximation for a shortwave radiative transfer model, *J. Quant. Spectrosc. Radiat. Transfer*, *62*, 109–121, 1999.

Kattawar, G. W., and C. N. Adams, Stokes vector calculations of the submarine light field in an atmosphere-ocean with scattering according to Rayleigh phase matrix: Effect of interface refractive index on radiance and polarization, *Am. Soc. Limnology Oceanogr.*, *34*, 1453–1472, 1989.

Koepke, E., Effective reflectance of oceanic whitecaps, *Appl. Opt.*, *23*, 1816–1824, 1984.

Kummerow, C., W. Barnes, T. Kozu, J. Shiue, and J. Simpson, The tropical rainfall measuring mission (TRMM) sensor package, *J. Atmos. Oceanic Technol.*, *15*, 809–817, 1998.

Lacis, A. A., J. Chowdhary, M. I. Mishchenko, and B. Cairns, Modeling errors in diffuse-sky radiation, vector versus scalar treatment, *Geophys. Res. Lett.*, *25*, 135–138, 1998.

Li, X., S. A. Christopher, J. Chou, and R. M. Welch, Estimation of shortwave direct radiative forcing of biomass burning aerosols using angular dependence models, *J. Appl. Meteorol.*, *39*, 2278–2291, 2000.

Loeb, N. G., and S. Kato, Top-of-atmosphere direct radiative effect of aerosols from the clouds and the Earth's radiant energy system satellite instrument (CERES), *J. Clim.*, *15*, 1474–1484, 2002.

Loeb, N. G., K. J. Priestley, D. P. Kratz, E. B. Geier, R. N. Green, B. A. Wielicki, P. O'R. Hinton, and S. K. Nolan, Determination of unfiltered radiances from the Clouds and the Earth's Radiant Energy System (CERES) instrument, *J. Appl. Meteorol.*, *40*, 822–835, 2001.

Loeb, N. G., S. Kato, and B. A. Wielicki, Defining top-of-atmosphere flux reference level for Earth radiation budget studies, *J. Clim.*, in press, 2002.

Long, C. N., and T. P. Ackerman, Identification of clear skies from broadband pyranometer measurements and calculation of downwelling shortwave cloud effects, *J. Geophys. Res.*, *105*, 15,609–15,626, 2000.

McClatchey, R. A., R. W. Fenn, J. E. A. Selby, F. E. Volz, and J. S. Garing, *Optical Properties of the Atmosphere*, 3rd ed., *Environ Res. Pap.*, vol. 411, 110 pp., Air Force Cambridge Res. Lab., Bedford, Mass., 1972.

Meador, W. E., and W. R. Weaver, Two-stream approximation to radiative transfer in planetary atmospheres: A unified description of existing methods and new improvement, *J. Atmos. Sci.*, *37*, 630–643, 1980.

Minnis, P., D. F. Young, B. A. Wielicki, P. W. Heck, X. Dong, L. L. Stowe, and R. Welch, CERES cloud properties derived from multispectral VIRS

data, paper presented at the EOS/SPIE Symposiumon Remote Sensing, Florence, Italy, 20–24 Sept. 1999.

Mishchenko, M. I., A. A. Lacis, and L. D. Travis, Errors induced by neglect of polarization in radiance calculations for Rayleigh-scattering atmosphere, *J. Quant. Spectrosc. Radiat. Transfer*, *51*, 491–510, 1994.

Morel, A., Optical modeling of the upper ocean in relation to its biogenous matter content (case 1 waters), *J. Geophys. Res.*, *93*, 10,749–10,768, 1988.

Nakajima, T., and M. Tanaka, Effect of wind-generated waves on the transfer of solar radiation in the atmosphere-ocean system, *J. Quant. Spectrosc. Radiat. Transfer*, *29*, 521–537, 1983.

Nakajima, T., and M. Tanaka, Algorithms for radiative intensity calculations in moderately thick atmospheres using a truncation approximation, *J. Quant. Spectrosc. Radiat. Transfer*, *40*, 51–69, 1988.

Plass, G. N., and G. W. Kattawar, Calculation of reflected and transmitted radiance for Earth's atmosphere, *Appl. Opt.*, *7*, 1129–1135, 1968.

Press, W. H., S. A. Teukolsky, W. T. Vetterling, and B. P. Flannery, *Numerical Recipes in FORTRAN*, 2nd ed., pp. 184–191, Cambridge Univ. Press, New York, 1992.

Priestley, K. J., B. R. Barkstrom, R. B. Lee, III, R. N. Green, S. Thomas, R. S. Wilson, P. L. Spence, J. Paden, and D. K. Pandey, Post launch radiometric validation of the Clouds and the Earth's Radiant Energy System (CERES) proto-flight model on the Tropical Rainfall Measuring Mission (TRMM) spacecraft through 1999, *J. Appl. Meteorol.*, *39*, 2249–2258, 2000.

Raschke, E., Multiple scattering calculation of the transfer of solar radiation in an atmosphere-ocean system, *Contrib. Atmos. Phys.*, *45*, 1–19, 1972.

Satheesh, S. K., and V. Ramanathan, Large differences in tropical aerosol forcing at the top of the atmosphere and Earth's surface, *Nature*, *405*, 60–63, 2000.

Stamnes, K., S.-C. Tsay, W. Wiscombe, and I. Laszlo, DISORT, a general-purpose fortran program for discrete-ordinate-method radiative transfer in scattering and emitting layered media: Documentation of methodology, ftp://climate.gsfc.nasa.gov/pub/wiscombe/Multiple_Scatt/, 2000.

Stowe, L. L., P. A. Davis, and E. P. McClain, Scientific bases and initial evaluation of the CLAVR-1 global clear/cloud classification algorithm for Advanced Very High Resolution Radiometer, *J. Atmos. Oceanic Technol.*, *16*, 656–681, 1999.

Takashima, T., and K. Masuda, Degree of radiance and polarization of the upwelling radiation from and atmosphere-ocean system, *Appl. Opt.*, *24*, 2423–2429, 1985.

Tanaka, M., and T. Nakajima, Effects of oceanic turbidity and index of refraction of hydrosols on the flux of solar radiation in the atmosphere-ocean system, *J. Quant. Spectrosc. Radiat. Transfer*, *18*, 93–111, 1977.

Toon, O. B., and J. B. Pollack, The optical constants of several atmospheric aerosol species: Ammonium sulfate, aluminum oxide and sodium chloride, *J. Geophys. Res.*, *81*, 5733–5748, 1976.

Trepte, Q., Y. Chen, S. Sun-Mack, P. Minnis, D. F. Young, B. A. Baum, and P. W. Heck, Scene identification for the CERES cloud analysis subsystem, paper presented at AMS 10th Conference, Atmospheric Radiation, Am. Meterol. Soc., Madison, Wis., 28 June to 2 July 1999.

Twomey, S., *Atmospheric Aerosols*, 280 pp., Elsevier Sci., New York, 1977.

van de Hulst, H. C., *Multiple Light Scattering, Tables, Formulas, and Applications*, vol. 2, Academic, San Diego, Calif., 1980.

Vermote, E. F., D. Tanré, and J.-J. Morcrette, Second simulation of the satellite signal in the solar spectrum, 6S: An overview, *IEEE Trans. Geosci. Remote Sens.*, *35*, 675–686, 1997.

Wauben, W. M. F., J. F. de Hann, and J. W. Hovenier, A method for computing visible and infrared polarized monochromatic radiation in planetary atmosphere, *Astron. Astrophys.*, *282*, 277–290, 1994.

Wielicki, B. A., B. R. Barkstrom, E. F. Harrison, B. B. Lee III, G. L. Smith, and J. E. Cooper, Clouds and the Earth's Radiant Energy System (CERES): An Earth observing system experiment, *Bull. Am. Meteorol. Soc.*, *77*, 853–868, 1996.

S. Kato and N. G. Loeb, Atmospheric Sciences, Mail Stop 420, NASA Langley Research Center, Hampton, VA 23681-2199, USA. (s.kato@larc.nasa.gov; n.g.loeb@larc.nasa.gov)

C. K. Rutledge, Analytical Services & Materials, Inc., Hampton, VA 23681-2199, USA. (c.k.rutledge@larc.nasa.gov)